https://doi.org/10.52131/jmps.2022.0302.0030

Journal of Materials and Physical Sciences

Volume 3, Number 2, 2022, Pages 96 - 108

Journal Homepage:
https://journals.internationalrasd.org/index.php/jmps

JOURNAL OF MATERIALS AND PHYSICAL SCIENCES
INTERNATIONAL RESEARCH ASSOCIATION FOR SUSTAINABLE DEVELOPMENT

Synthesis and Characterization of Rare Earth Doped Ferrite / Polyethylene Oxide Nanocomposites

Muhammad Ishfaq[1], Mahvish Gul[2], Hatem Alamri[3], Gulfam Nasar[4*], Faseeh ur Raheem[5]

[1] Govt. Graduate College Chishtian, Bahawalnagar, Pakistan
[2] Department of Chemistry, The Islamia University of Bahawalpur, Bahawalpur 63100, Pakistan
[3] Umm Al-Qura University Makkah, Saudi Arabia
[4] Department of Chemistry, Balochistan University of Information Technoogy, Engineering and Management Sciences, Quetta, Pakistan
[5] Institute of Physics, The Islamia University of Bahawalpur, Bahawalpur, Pakistan

ARTICLE INFO

Article History:
Received: November 19, 2022
Revised: December 15, 2022
Accepted: December 30, 2022
Available Online: December 31, 2022

Keywords:
Ferrite-Polymer Nanocomposites
Polyethylene Oxide
FTIR
XRD
Dielectric Properties
SEM

ABSTRACT

Nano-sized $Li_{0.5}Ni_{0.48}Tb_{0.02}Dy_{0.1}Fe_{1.9}O_4$ spinel ferrite nanoparticles were synthesized employing the micro-emulsion synthesis method. Polyethylene oxide was prepared through in-situ polymerization route. The ferrite-polymer nanocomposites have been synthesized by combining $Li_{0.5}Ni_{0.48}Tb_{0.02}Dy_{0.1}Fe_{1.9}O_4$ ferrite with polyethylene oxide polymer. Spectral, structural, morphological, and dielectric properties of the prepared nano-ferrite powders as well as nanocomposites were investigated by "X-ray diffraction analysis" (XRD), "scanning electron microscopy" (SEM), "Fourier transform infrared spectroscopy" (FTIR) and dielectric measurements. XRD analysis confirmed the synthesis of single-phase spinel structure only. The dielectric parameter was augmented with an increase of ferrite amount. FTIR spectra confirmed the existence of interactions between polyethylene oxide and ferrite particles. SEM study revealed that the nanocomposites comprised core/shell structure and inhomogeneous distribution of grain size. The dielectric parameters such as "real part of dielectric constant" (ἐ), "imaginary part of dielectric constant" (ε"), "tan loss", "AC conductivity" and "quality factor" were investigated in the required range of frequency; that is, 1 MHz – 3 GHz. The peaking behavior has been observed for real (ε') and "imaginary (ε'') parts of dielectric constant" and "dielectric loss" (tanδ). "The peaking behavior" was detected beyond 1.5 GHz. A decrease in "the dielectric constants" and "dielectric loss" was found to with the increasing frequency. Dielectric parameters have been well elucidated by explaining "Debye-type relaxation model" in agreement with two layer "Koop's phenomenological theory". The present investigated samples might have potential applications in high frequency.

*Corresponding Author's Email: gulfam.nasar@buitms.edu.pk

1. Introduction

Ferrites and oxides possess magnetic properties which have been a matter of great interest and have been studied extensively (Rinkevich, Korolev, Samoylovich, Klescheva, & Perov, 2016). Magnetic properties of the oxide nanoparticles are elucidated to set up a logical connection between the magnetic behavior and the nanoscale size. Super-paramagnetic properties have been observed by the magnetite nanoparticles prepared at the room temperature by co-precipitation method (Kim & Shima, 2007). Magnetic oxides are applied effectively in a variety of technological fields, including water treatment and

environmental protection. Using this technique, huge amount of water can be treated in a relatively very short time and more effectively (Qi, Huang, Yan, Li, & Pan, 2015). The nanocomposites of "zinc ferrite-reduced graphene oxide" (ZF-rGO) have been able to remove toxic contaminations very effectively using their high adsorption capability. The adsorption of a magnetic ferrite is attributed to its enhanced magnetic properties (Fei, Wang, Zhong, & Su, 2016). The applicability of nanomaterials could possibly be enhanced by varying the nanoparticles' size(Nasar et al., 2016). The size of nanoparticles has a direct connection with the physical properties (Choudhry et al., 2015). Perovskites (the metal oxides with general formula ABO_3) have been found very useful in several technological applications due to their unique properties (Kammer Hansen, 2013; Li, Qiu, Wang, Jiang, & Xu, 2008).

Polymer nanocomposites with magnetic materials form a prominent class of material science, in which nanoparticles of magnetic materials are entrenched in polymer matrix (Ahmed, Okasha, Mansour, & El-dek, 2010). The nanocomposites thus formed possess a great capability of applications like electromagnetic interference suppression, drug discharge (Yinglin et al., 2014), industrial automatization (Cheng, Zhang, Yi, Ye, & Xia, 2008) and electromagnetic devices (Varshney et al., 2012). Polymer- ferrite nanocomposites have been finding special attention due to their wider applicability in various advanced devices; for example fuel cell (Ahmed et al., 2010), high performance batteries (Salafsky, 1999) , supercapacitor (Awadhia, Patel, & Agrawal, 2006) and sensors (Ashis, Sukanta, Amitabha, & De, 2004). Polymers serve as preferable matrix due to their binding properties and stabilization (Awadhia et al., 2006). Polymer matrix can build up a good interaction with ferrite nanoparticles and this interaction is attributed to formation of chemical or temporary bonds e.g., hydrogen bonding between the two components of the composite material. Normally extend of magnetization of the nanocomposite has an inverse relation with the ferrite concentration (Sankara Rao et al., 2015). The magnetic properties of given nanocomposites are altered by varying the concentration of the ferrites (Azhar Khan et al., 2015).

Quite a large number of scientific studies have been reported on ferrite-polymer nanocomposites such as Sm substituted lithium nickel ferrite-polyaniline nanocomposites as soft magnetic material (Li, Jiang, & Xu, 2007), Polyaniline-LiNi ferrite composites synthesized by in situ polymerization of aniline (Jiang, Li, & Xu, 2007), cobalt ferrite/polyvinyl alcohol nanocomposites (Mirzaee, Farjami Shayesteh, & Mahdavifar, 2014), cobalt ferrites nanoparticles with polymethyl methacrylate (PMMA) (Hannour et al., 2014) have been studied theoretically and experimentally. The ferrite polymer composites with varying compositions of ferrites or matrices have been synthesized using polymers, co-polymers, conducting (Feller, Bruzaud, & Grohens, 2004) and non-conducting (Seo, Rhee, & Park, 2011) polymers including crystalline (Castel et al., 2009) and amorphous fillers (Abbas, Dixit, Chatterjee, & Goel, 2007). These composites exhibited very auspicious properties which make them fit to be used in electrical applications, as effective EMI shielding materials (Huang et al., 2007), medical instruments, radar system, high-speed wireless systems, satellite communications etc. (Bueno, Gregori, & Nóbrega, 2008).

Till now, various composites have been used for variety of applications. However, rare earth doped Li-Ni ferrite ($Li_{0.5}Ni_{0.48}Tb_{0.02}Dy_{0.1}Fe_{1.90}O_4$) with polyethylene oxide polymer is not discussed. In present work, micro-emulsion method was employed to synthesize $Li_{0.5}Ni_{0.48}Tb_{0.02}Dy_{0.1}Fe_{1.90}O_4$ ferrite and "in situ polymerization method" was taken into consideration to prepare ferrite-polymer nanocomposites. In this study we have explored the effects of ferrite concentration in the polymer matrix on the structural, morphological, spectral, and dielectric properties of lithium-nickel rare earth doped ferrite-polymer nanocomposites. The main aim of the current research is to explain the usefulness of the nanocomposites in high frequency devices applications.

2. Experimental Procedure

2.1. Materials

Lithium chloride, Nickel (II) Chloride Hexahydrate, Terbium Heptoxide, Dysprosium Nitrate Hydrate, Iron (III) Chloride, Cetyltrimethylammonium bromide (CTAB), Aqueous Ammonia and de-ionized water.

2.2. Synthesis of $Li_{0.5}Ni_{0.48}Tb_{0.02}Dy_xFe_{2-x}O_4$ Nanoparticles

Different amounts of metal salt solutions were added to form various compositions of $Li_{0.5}Ni_{0.48}Tb_{0.02}Dy_xFe_{2-x}O_4$, where x = 0, 0.05, 0.1, 0.15, 0.2. Appropriate concentration of salt solutions of Li, Ni, Tb, Dy and Fe were prepared and mixed with magnetic stirrer at 50-60 °C. 0.3 Molar aq. solution of CTAB was added to this mixture. The pH of prepared solution was sustained up to a level of 10 by a continuous slow addition of aqueous solution of ammonia. Thereafter, all samples were stirred for six hours and were kept overnight to ensure complete settling down of the precipitates, which were later washed using "de-ionized water" until pH ~ 7 was attained. The washed contents were heat dried and ground followed by annealing for eight hours at 980 °C to remove any possible traces of CTAB and impurities of organic compounds.

2.3. Preparation of Nanocomposites

Initially, 60 ml water was heated in a beaker at 50 °C and 1g pre-weighed polyethylene oxide was added slowly into it with continuous and vigorous stirring for three hours. At this stage 0.1, 0.2, 0.3, 0.4 and 0.5 g pre-weighed ferrite was added slowly into solution, with continuous stirring. The temperature of homogenous solution was kept at 60 °C along with steady stirring to obtain thick gel of polymer nanocomposites. The gels were converted into films by evaporation at room temperature in a petri dish. On drying, films were detached from the petri plates for characterization.

2.4. Characterization Techniques

The measured XRD plots of $Li_{0.5}Ni_{0.48}Tb_{0.02}Dy_xFe_{2-x}O_4$ nano-structured ferrite and their nano-composites were recorded on diffractometer model "Philips-X" Pert-PRO 3040 / 60" taking Copper-K_α as "primary source of radiation" to examine the development of phase of the prepared materials. Average crystallite size (D) of the given prepared nanomaterials inspected on the basis of "line broadening peaks of X-ray diffraction" and determined through the "Scherrer's formula":

$$D = K\lambda / \beta \cos\theta \quad (1)$$

Here D labels the "average size of crystallite" of the particles under examination, K is the "Scherrer's constant" is equal to 0.89, λ denotes to the wavelength of applied X-ray beam" used, β corresponds to the "full-width at half maxima of XRD peaks" (FWHM) and θ = "Bragg's angle of diffraction" (Cullity, 1978). "Fourier transformation infrared spectroscopy" (FTIR) was employed using "Tensor 27 spectrometer". The spectra of FTIR were used to determine all types of organic, functional groups in organic materials, various types of inorganic compounds and molecular composition of surfaces. All frequencies are simultaneously observed by FTIR spectroscopy (Griffiths, 1986).

The morphological studies of ferrite-polymer nanocomposites were executed using electron scope Model: "Jeol JSM- 6490A". The purpose of the SEM examination was to know their surface morphology and to make an estimation of particle size. The dielectric measurement was performed and evaluated using "4287/ARF LCR meter" for frequency ranges from 1 MHz to 3 GHz. The dielectric behavior of the synthesized samples was investigated as a function of frequency and concentration. The frequency range was 1MHz-3GHz. Every material has unique electrical characteristics and it depends on its dielectric properties, which are significant for designing the material for specific application (Goldman, 1990).

3. Results and Discussion

3.1. Structural Analysis

"X-ray diffraction patterns" of $Li_{0.5}Ni_{0.48}Tb_{0.02}Dy_{0.0.02}Fe_{1.9}O_4$ ferrite/polyethylene oxide (PEO) nanocomposites are shown in Fig.1. The compositions of all the samples under investigation and their ferrite-polymer ratios are tabulated in Table 1. All these peaks were clearly matched and confirmed the "single phase spinel structure" using the results of X-ray diffraction. The peak with the maximum intensity of all sample is identified with hkl (311)

(Ali et al., 2014). The secondary trace of ortho-rhombic phase is appeared at 33° (labeled by * in Fig 1) which is identified as $DyFeO_3$. The appearance of secondary peak is attributed to excess of Dy^{3+} ions because it possesses larger ionic radii than that of the host ions. The results revealed that substitution of little amount of Dy^{+3} ions into the structure of spinel ferrites replace ferric Fe^{3+} ions on the "octahedral-sites" obeying the Vegard's law. The average lattice constant was observed to 8.329 Å. The calculated crystallite size lies within the range 34-47 nm. The lithium and nickel ions have preference to go "tetrahedral sites" and ferric Fe^{3+} ions are disseminated between "tetrahedral and octahedral sites" (Al-Hilli, Li, & Kassim, 2009).

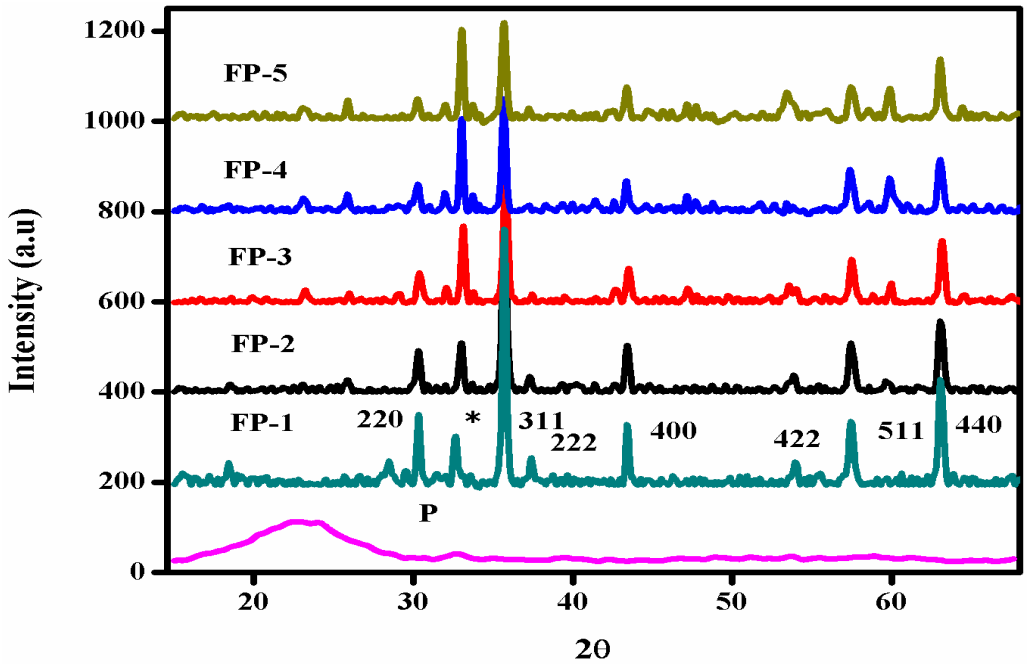

Figure 1: XRD patterns of $Li_{0.5}Ni_{0.48}Tb_{0.02}Dy_{0.0.02}Fe_{1.9}O_4$ ferrite/PEO nanocomposites

"Nelson-Riley function" was empyed to find out the average value of "lattice constant" (a). The average lattice constant of $Li_{0.5}Ni_{0.48}Tb_{0.02}Dy_{0.0.02}Fe_{1.9}O_4$ ferrite/PEO nanocomposites is found to increase from 8.329- 8.349 Å. The increase in (a) has been explained with respect to ionic radii of cations. The ionic radii of dopants such as of terbium (0.93 Å) and dysprosium (0.912Å) are larger than that of host cations; ferric ions (Fe^{3+} is 0.64 Å), (Li^{+1} is 0.74 Å) and (Ni^{2+} is 0.69 Å). The raise in lattice constant is owing to substitution of small-size ions with the larger ones (Azhar Khan et al., 2014; Ishaque et al., 2010).

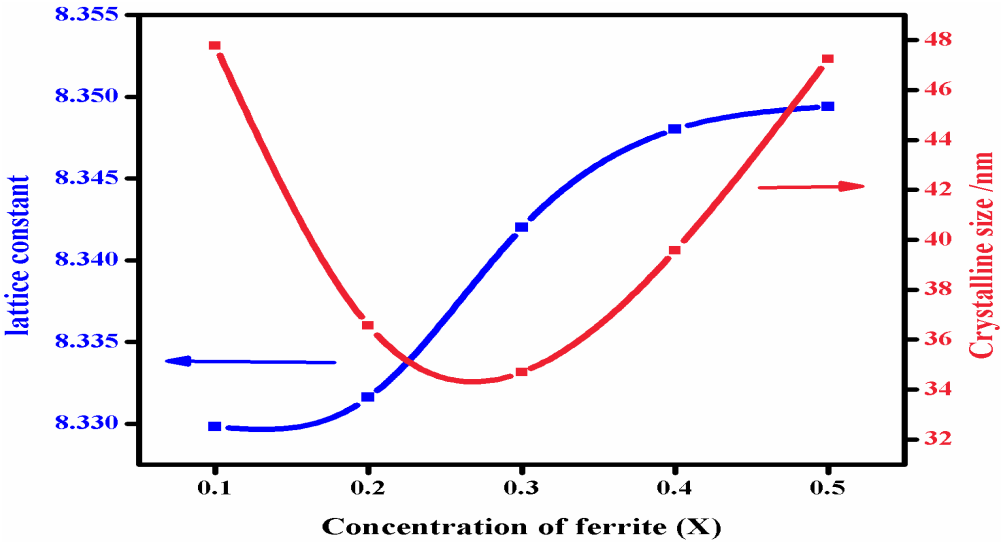

Figure 2: Lattice constant and crystallite size of $Li_{0.5}Ni_{0.48}Tb_{0.02}Dy_{0.02}Fe_{1.9}O_4$ ferrite/PEO nanocomposites

The average size of crystallite was deliberated by the Scherer's equation (Soibam, Phanjoubam, Sharma, Sarma, & Prakash, 2009). Initially the value of crystallite size of $Li_{0.5}Ni_{0.48}Tb_{0.02}Dy_{0.0.02}Fe_{1.9}O_4$ ferrite/PEO nanocomposites decreases and then it increases with an increase of ferrite concentration (Al-Hilli, Li, & Kassim, 2012). These variations are shown in Table 2 as well as in Fig. 2.

3.2. Spectral Analysis

The FTIR spectra of $Li_{0.5}Ni_{0.48}Tb_{0.02}Dy_{0.0.02}Fe_{1.9}O_4$ ferrite/PEO nanocomposites are measured in the range 500-4500 cm^{-1} and these are shown in Fig. 3 (a-e). FTIR bands detected in the range of 400-600 cm^{-1} are assigned to metal-oxygen stretching vibrations. The "absorption bands" which are in the given range 500-600 cm^{-1} are attributed as tetrahedral-sites (A) fundamental stretching vibration of metal-ions while the peaks appearing within 400-385 cm^{-1} are attributed as "octahedral sites (B) among the metal stretching vibrations" (Choodamani et al., 2013).

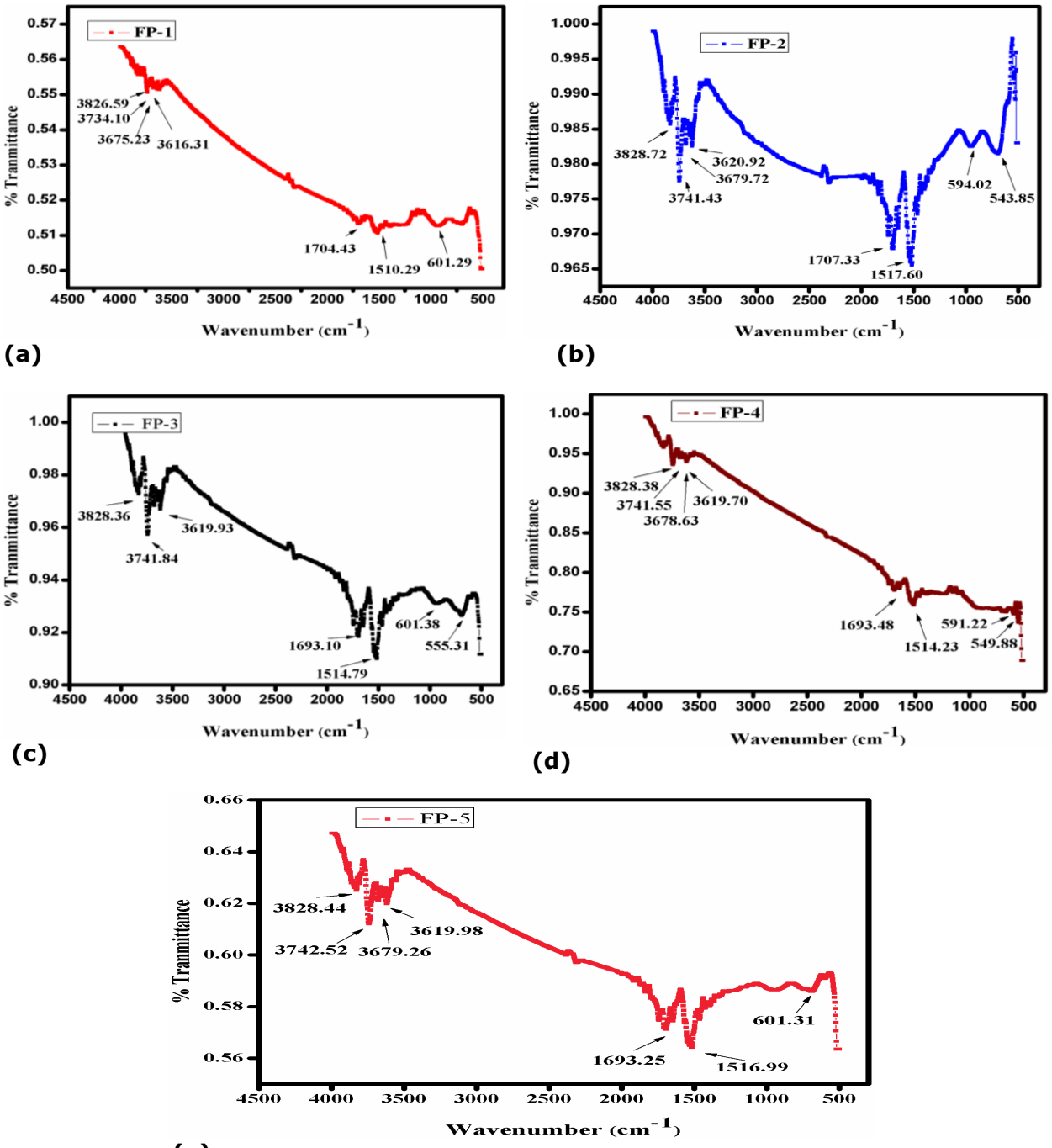

Figure 3: FTIR Spectra (a: $Li_{0.5}Ni_{0.48}Tb_{0.02}Fe_{1.90}O_4$, b: $Li_{0.5}Ni_{0.48}Tb_{0.02}Fe_{1.90}O_4$, c: $Li_{0.5}Ni_{0.48}Tb_{0.02}Fe_{1.90}O_4$, d: $Li_{0.5}Ni_{0.48}Tb_{0.02}Fe_{1.90}O_4$ e: $Li_{0.5}Ni_{0.48}Tb_{0.02}Fe_2O_4$)

Both mention fundamental bands attributed to the vibrations of octahedral and tetrahedral sites of cations in the spinel ferrites lattice. The appeared variation in the absorption location of tetrahedral and octahedral complexes of spinel arrangement is attributed to the diverse detachment between ferric-oxygen ions (Fe^{3+}–O^{2-}) in the tetrahedral and octahedral-sites (Srivastava, Ojha, Chaubey, Sharma, & Pandey, 2010). The peaks appeared in the range 1500-1700 cm^{-1} are due to the N-H and C = O vibrations of stretching. The spectra appeared above 3600 cm^{-1} are due to moisturizing and water molecules (Srivastava et al., 2014).

Table 1
The synthesized compositions of polymer, ferrite/polymer composites.

Sr. No.	Composition	Ferrite : Polymer Ratio
1	P	Polymer
2	FP1	0.1g : 1g
3	FP2	0.2g : 1g
4	FP3	0.3g : 1g
5	FP4	0.4g : 1g
6	FP5	0.5g : 1g

Table 2
Lattice parameter and crystallite size of ferrite/polymer nanocomposites

Ferrite concentration (X)	Lattice constant (a) Å	Crystallite size (D) nm
0.1	8.329	47.76
0.2	8.3316	36.56
0.3	8.342	34.70
0.4	8.348	39.57
0.5	8.349	47.24

3.3. Morphological Analysis

The "scanning electron micrographs" (SEM) is best for morphological analysis of $Li_{0.5}Ni_{0.48}Tb_{0.02}Dy_{0.0.02}Fe_{1.9}O_4$ ferrite/PEO nanocomposites are shown in Fig. 4 (a-c). The micrographs of nanocomposites indicate irregular size of the particles. A slight agglomeration of particles has been observed owing to the inter particles (particle-particle) interactions. Particles of Ferrite are monitored for uniform encapsulation with polymeric matrix which signifies the presence of the nano-crystalline ferrites into the medium of polymer. All SEM images exposed the confirmation of nano-sized structure in all compositions. An increase in the average crystallite size was observed with increasing ferrite content (Patil, Jadhav, & Hankare, 2013; Srivastava et al., 2010).

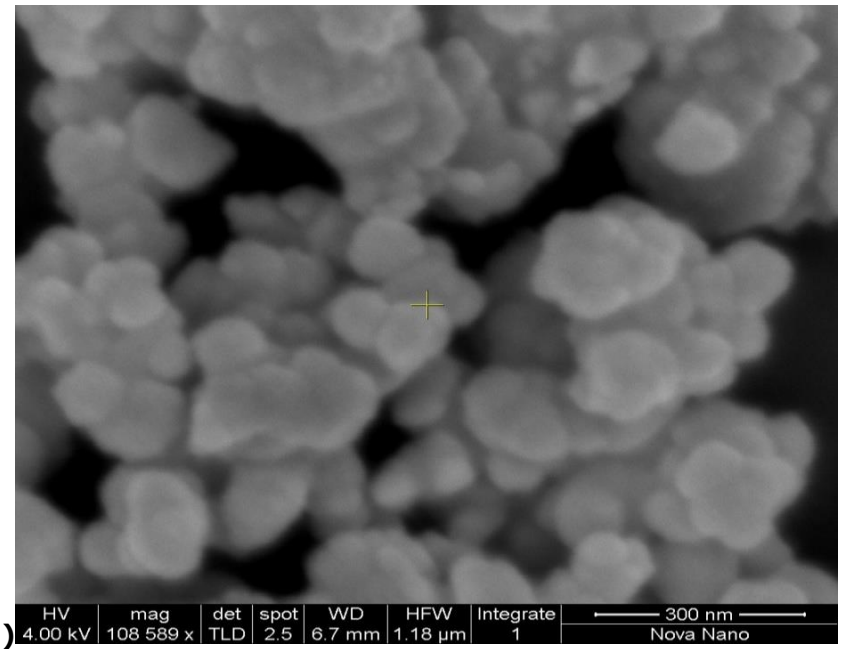

(a)

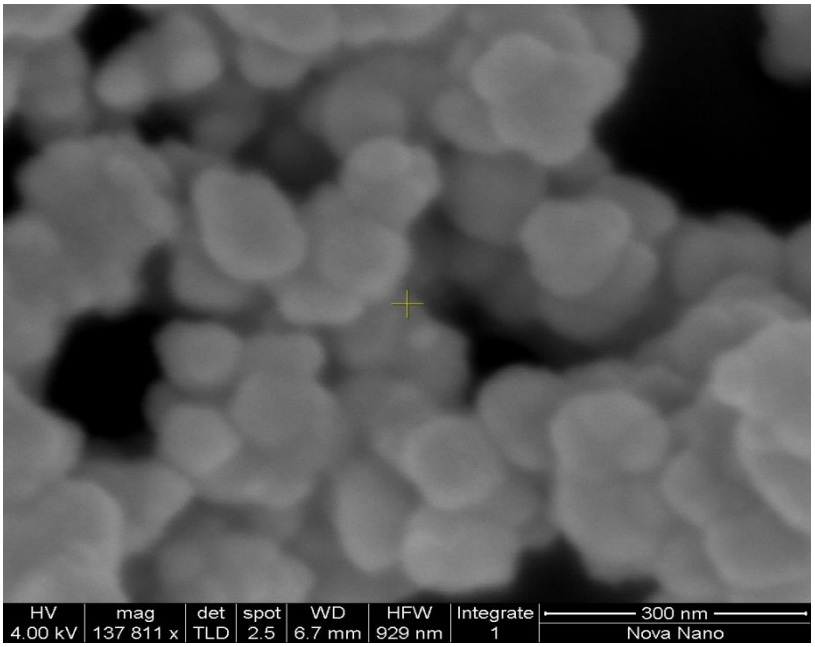

(b)

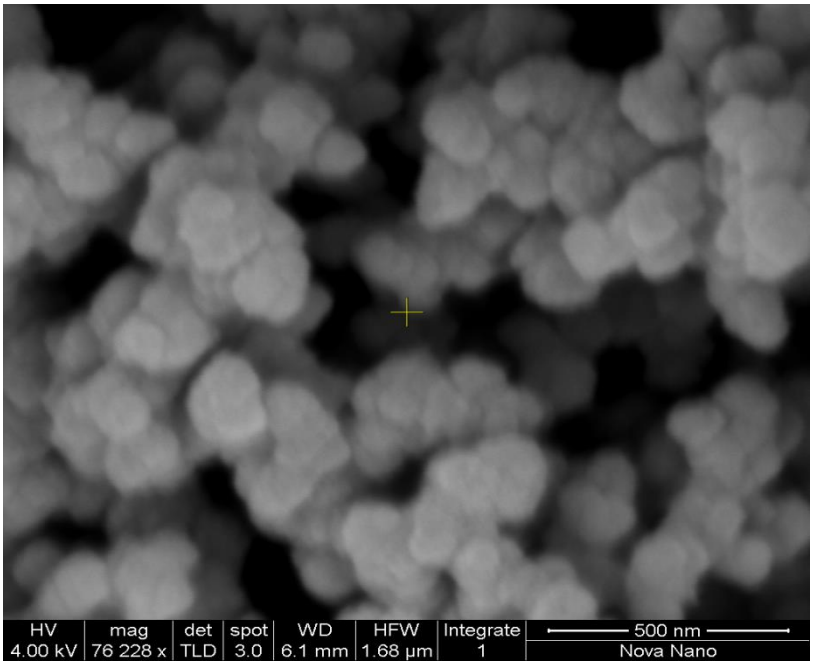

(c)

Figure 4: SEM micrograph of ferrite/PEO nanocomposites (a: $Li_{0.5}Ni_{0.48}Tb_{0.02}Fe_2O_4$ (FP 1), b: $Li_{0.5}Ni_{0.48}Tb_{0.02}Fe_2O_4$ (FP-3), c: $Li_{0.5}Ni_{0.48}Tb_{0.02}Fe_2O_4$ (FP-5))

3.4. Dielectric Properties for $Li_{0.5}Ni_{0.48}Tb_{0.02}Dy_{0.0.02}Fe_{1.9}O_4$ Ferrite

Figure 5 and 6 demonstrate the frequency dependent difference of "dielectric constant (real component)" and "dielectric loss (imaginary component)" respectively of $Li_{0.5}Ni_{0.48}Tb_{0.02}Dy_{0.0.02}Fe_{1.9}O_4$ ferrite/PEO nanocomposites taken at ambient temperature within 1 MHz-3 GHz. It is evident from the figures that both "dielectric loss" and "dielectric constant" exhibit dispersion with frequency. Both ε' and ε'' show increasing trend at lower frequency but decline quickly at larger frequency. This kind of behavior basically involves the spreading process due to "Maxwell-Wagner type interfacial polarization" which is in good agreement with two-layer "Koop's phenomenological model". The electron exchange phenomenon happening between ferrous Fe^{2+}/ ferric Fe^{3+} ions result in rearrangement of charges under the influence of an external applied electric field which is responsible for the electric polarization. The degree of polarization drops off with increasing the frequency and approaches a steady value because the variation of position of electrons between the two types of ferrous Fe^{2+}/ ferric Fe^{3+} ions cannot match with the alternating field further than a certain frequency limit. The interfacial as well as dipolar polarization participate at low frequency while contribution to hopping process at high frequency mainly comes from the electronic polarization.

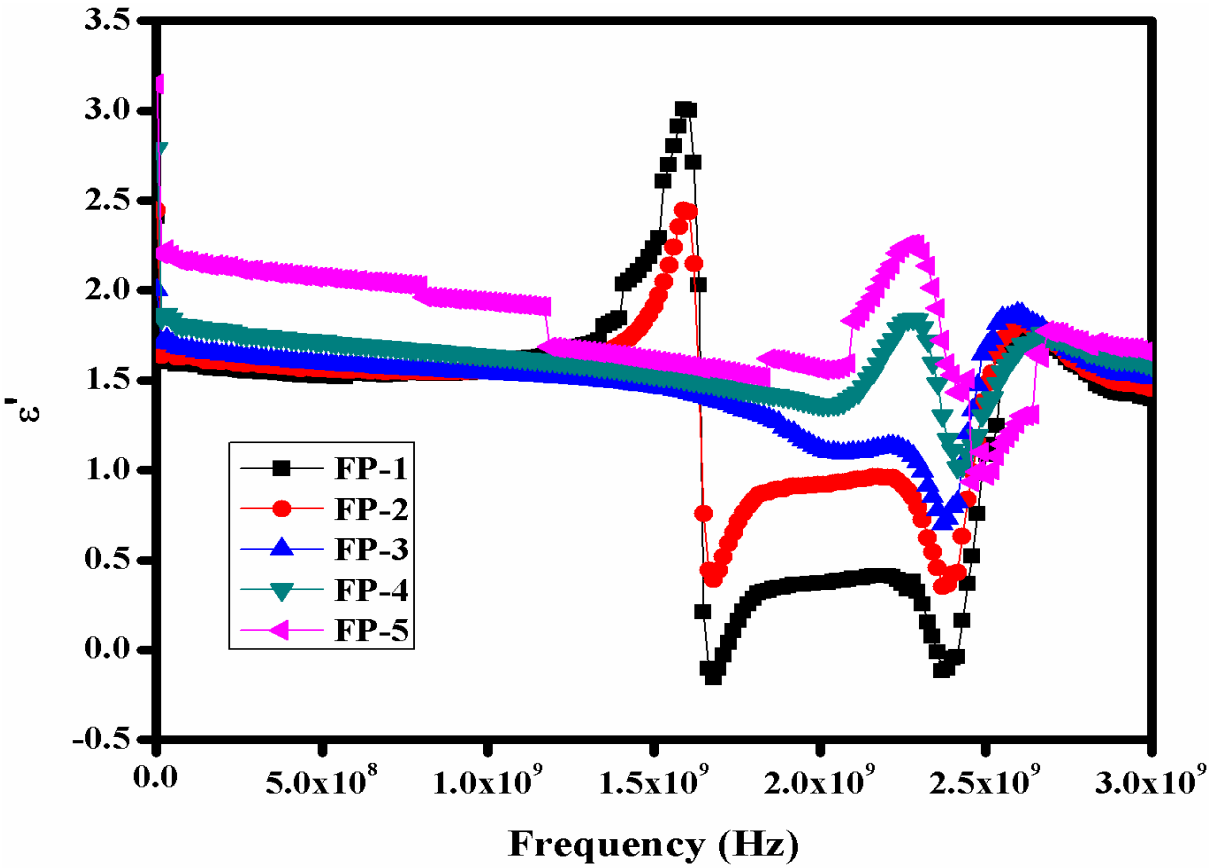

Figure 5: Dielectric constant of $Li_{0.5}Ni_{0.48}Tb_{0.02}Fe_{1.90}O_4$ ferrite/PEO nanocomposites

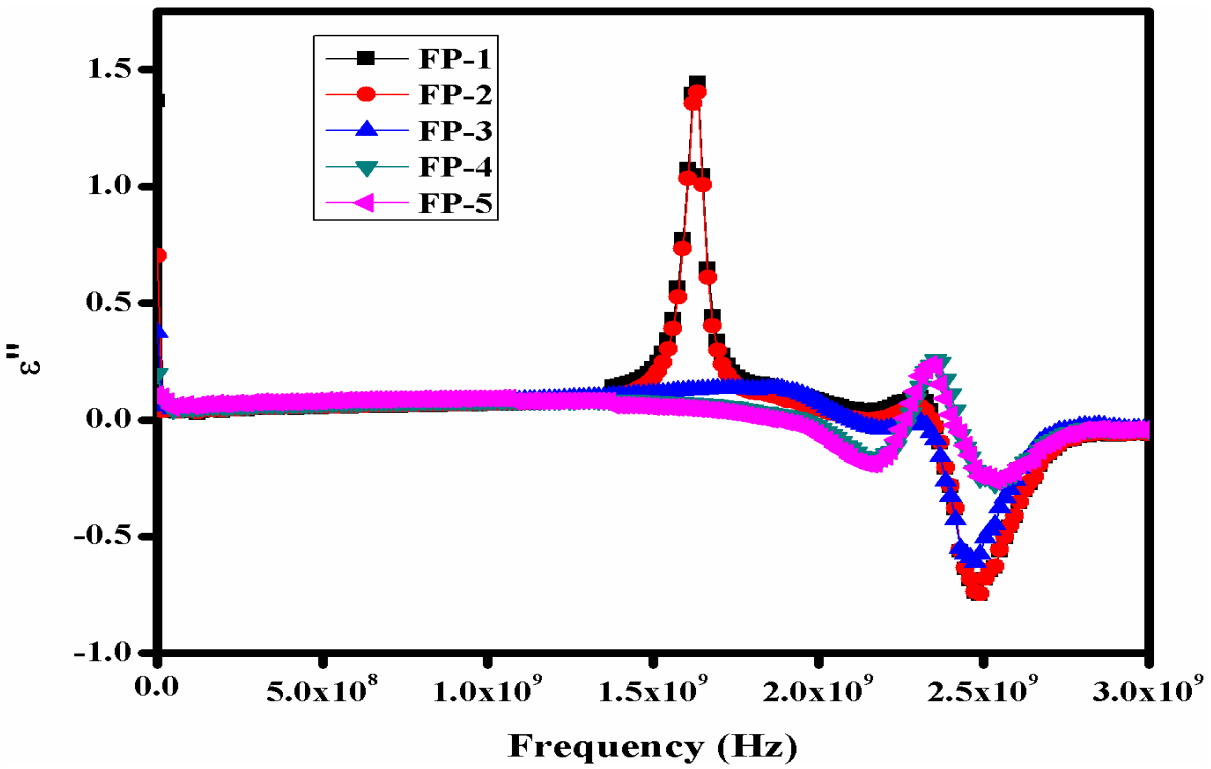

Figure 6: Dielectric loss of $Li_{0.5}Ni_{0.48}Tb_{0.02}Fe_{1.90}O_4$ ferrite/PEO nanocomposites

Several resonance peaks occurred at high frequency (f > 1.5 GHz) once the frequently electrons transfer between ferrous (Fe^{2+}) /ferric (Fe^{3+}) ions become equivalent to the frequency of external applied AC field which occurred due to un-damped dipoles. This type of phenomenon is termed as ferromagnetic resonance (Azhar Khan et al., 2014; Singh, Agarwal, & Sanghi, 2011). Generally, when an ion possesses two stable states E and F carrying some potential energies with them and separated through a potential barrier, then jumping probability on either side is the same for both ions. The frequency at which ions

change their polarity at any side is named as its natural frequency. The moment at which external applied field and natural frequencies become equivalent, highest amount of electrical energy is transferred to oscillating ion that increases power loss which caused the resonance effect and ultimately the shaping the resonance peaks (Asif Iqbal et al., 2014).

3.4.1.Loss Tangent

Fig. 7 displays the "dielectric loss factor" variation with frequency from 1 MHz-3 GHz for all ferrite-polymer nanocomposites. It is obvious from Fig. 7 that tanδ decreases with increasing the frequency. When the frequency of the externally applied ac electric field is much smaller as compared to the electrons hopping frequency between ferrous Fe^{2+}/ ferric Fe^{3+} ions then electrons can chase the applied field and as a resultant, loss is maximum. When the frequency of the externally applied electric field is high than the hopping frequency of the electron exchange between Fe^{3+}-Fe^{2+} ions, electrons cannot chase the applied field further than certain frequency limit resulting in a minimum loss. At lower frequency tanδ is high and tends to decrease quickly at larger frequency in agreement with Koop's phenomenological model. It is worth remembering that high energy loss is associated with small frequency region while this loss has low value for high frequency zone (Asif Iqbal et al., 2014).

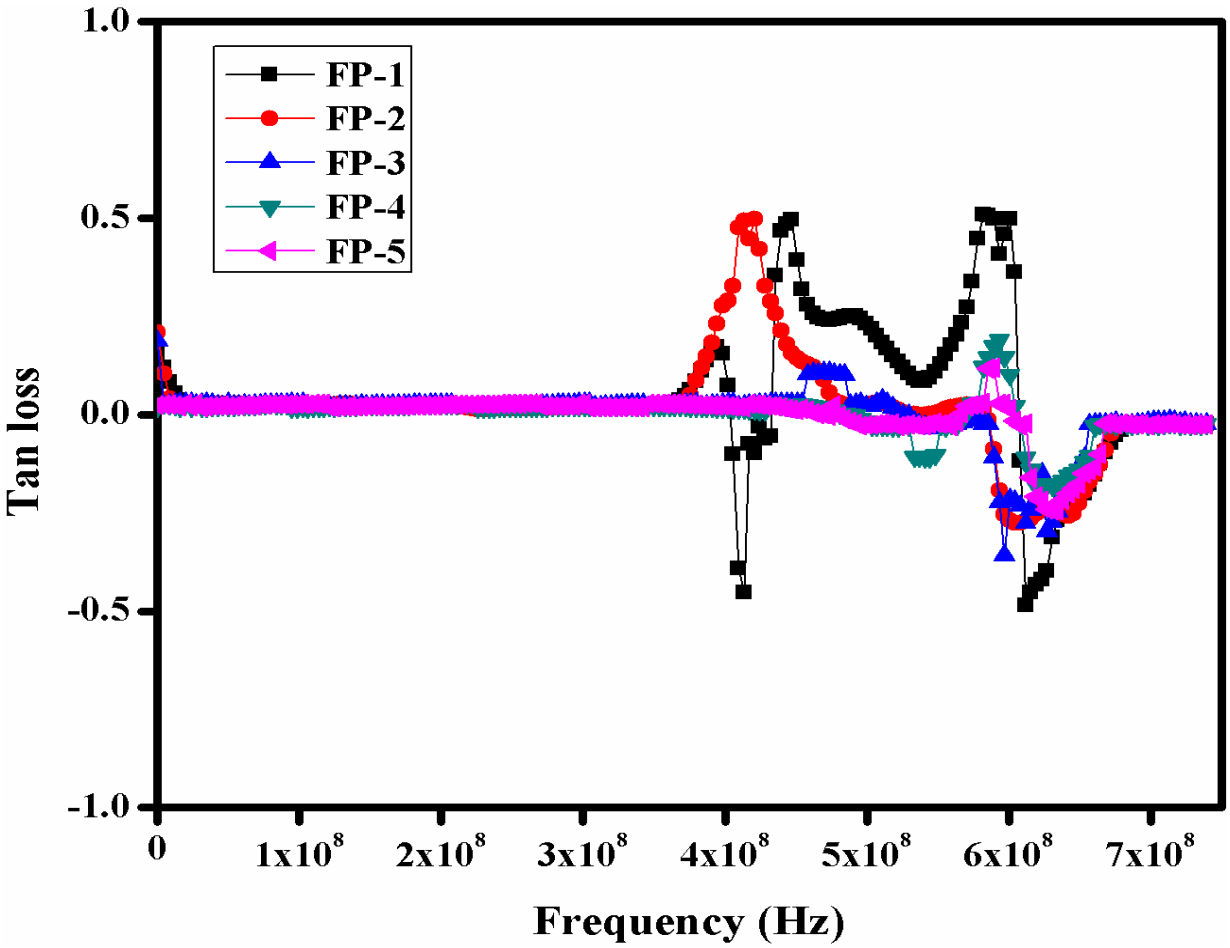

Figure 7: Tan loss of $Li_{0.5}Ni_{0.48}Tb_{0.02}Fe_{1.90}O_4$ ferrite/PEO nanocomposites

Figure 8 reveals the deviation in conductivity behavior for all samples of ferrite-polymer nanocomposites. The AC conductivity plots indicate that all compositions follow a rising behavior at lesser frequency area whereas dispersion takes place at a greater frequency zone. The "two-layer of the ferrite composites comprise of well conducting grains, alienated from each other through a thin layer of resistive grain boundaries explained by Koop's and "Maxwell-Wagner model. Both dielectric polarization and conduction procedure are coupled to each other. Grains play dominant role at higher frequency and hopping rate between ferrous Fe^{2+}/ ferric Fe^{3+} ions get increased owing to this phenomenon, therefore the ac electrical conductivity increased (Asif Iqbal et al., 2014).

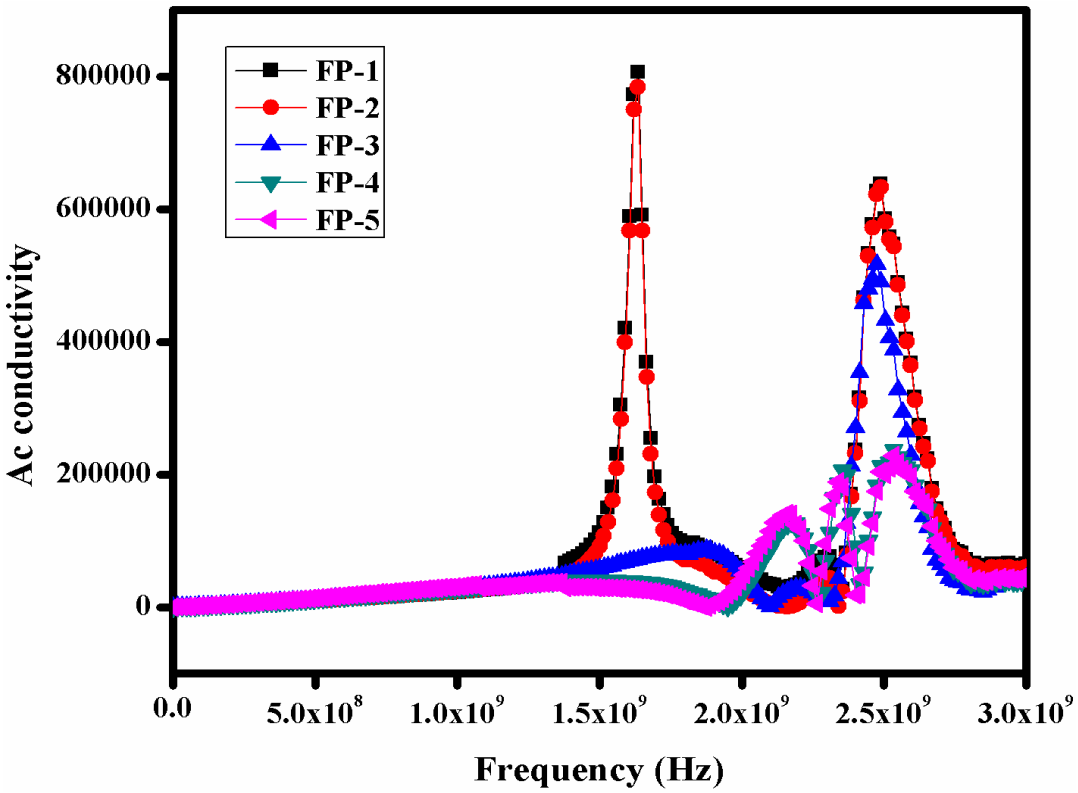

Figure 8: Ac conductivity of $Li_{0.5}Ni_{0.48}Tb_{0.02}Fe_{1.90}O_4$ ferrite/PEO nanocomposites

Conclusion

$Li_{0.5}Ni_{0.48}Tb_{0.02}Dy_{0.10}Fe_{1.90}O_4$ ferrite/polyethylene oxide nanocomposites were produced by chemical process. XRD spectra revealed that the produced peaks attributed to FCC spinel structure except at 33°. The size of crystallites was measured using "Scherrer's equation". The calculated crystallites size lies in 34-47 nm range. FTIR spectra show solid interactions between these ferrite nanoparticles and Polymers. Scanning electron microscopy revealed heterogeneous grain size distribution. The dielectric parameters were optimized by raising the amount of ferrite fraction of the composite materials. All the samples (FP1- FP5) exhibit peaking behavior. These nanocomposites exhibit resonance phenomenon in the high frequency range (GHz). The "dielectric constant" reduces with raising the frequency in the nanocomposite samples. A peaking behavior is observed for all the samples at 1.6 GHz and 2.4 GHz. The rate of tangent loss also falls with increasing frequency. A resonance phenomenon in the frequency range 1.65-3 GHz is observed for FP1-FP5. The measurement of "dielectric constant" and "tangent loss" with frequency of the applied field and doping concentration of rare earth doped Li-Ni ferrite in polyethylene oxide suggest suitability of these ferrite-polymer-nanocomposites in high frequency applications.

References

Abbas, S. M., Dixit, A. K., Chatterjee, R., & Goel, T. C. (2007). Complex permittivity, complex permeability and microwave absorption properties of ferrite–polymer composites. *Journal of Magnetism and Magnetic Materials, 309*(1), 20-24. doi:http://dx.doi.org/10.1016/j.jmmm.2006.06.006

Ahmed, M. A., Okasha, N., Mansour, S. F., & El-dek, S. I. (2010). Bi-modal improvement of the physico-chemical characteristics of PEG and MFe2O4 subnanoferrite. *Journal of Alloys and Compounds, 496*(1–2), 345-350. doi:http://dx.doi.org/10.1016/j.jallcom.2010.02.009

Al-Hilli, M. F., Li, S., & Kassim, K. S. (2009). Microstructure, electrical properties and Hall coefficient of europium-doped Li–Ni ferrites. *Materials Science and Engineering: B, 158*(1–3), 1-6. doi:http://dx.doi.org/10.1016/j.mseb.2008.12.022

Al-Hilli, M. F., Li, S., & Kassim, K. S. (2012). Structural analysis, magnetic and electrical properties of samarium substituted lithium–nickel mixed ferrites. *Journal of*

Magnetism and Magnetic Materials, 324(5), 873-879. doi:http://dx.doi.org/10.1016/j.jmmm.2011.10.005

Ali, R., Mahmood, A., Khan, M. A., Chughtai, A. H., Shahid, M., Shakir, I., & Warsi, M. F. (2014). Impacts of Ni–Co substitution on the structural, magnetic and dielectric properties of magnesium nano-ferrites fabricated by micro-emulsion method. *Journal of Alloys and Compounds, 584*(0), 363-368. doi:http://dx.doi.org/10.1016/j.jallcom.2013.08.114

Ashis, D., Sukanta, D., Amitabha, D., & De, S. K. (2004). Characterization and dielectric properties of polyaniline–TiO 2 nanocomposites. *Nanotechnology, 15*(9), 1277.

Asif Iqbal, M., Islam, M. U., Ali, I., khan, M. A., Sadiq, I., & Ali, I. (2014). High frequency dielectric properties of Eu+3-substituted Li–Mg ferrites synthesized by sol–gel auto-combustion method. *Journal of Alloys and Compounds, 586*(0), 404-410. doi:http://dx.doi.org/10.1016/j.jallcom.2013.10.066

Awadhia, A., Patel, S. K., & Agrawal, S. L. (2006). Dielectric investigations in PVA based gel electrolytes. *Progress in Crystal Growth and Characterization of Materials, 52*(1–2), 61-68. doi:http://dx.doi.org/10.1016/j.pcrysgrow.2006.03.009

Azhar Khan, M., Riaz, S., Ali, I., Niaz Akhtar, M., Murtaza, G., Ahmad, M., . . . Farooq Warsi, M. (2015). Structural and magnetic behavior evaluation of Mg–Tb ferrite/polypyrrole nanocomposites. *Ceramics International, 41*(1, Part A), 651-656. doi:http://dx.doi.org/10.1016/j.ceramint.2014.08.117

Azhar Khan, M., Sabir, M., Mahmood, A., Asghar, M., Mahmood, K., Afzal Khan, M., . . . Farooq Warsi, M. (2014). High frequency dielectric response and magnetic studies of Zn1−xTbxFe2O4 nanocrystalline ferrites synthesized via micro-emulsion technique. *Journal of Magnetism and Magnetic Materials, 360*(0), 188-192. doi:http://dx.doi.org/10.1016/j.jmmm.2014.02.059

Bueno, A. R., Gregori, M. L., & Nóbrega, M. C. S. (2008). Microwave-absorbing properties of Ni0.50−xZn0.50−xMe2xFe2O4 (Me=Cu, Mn, Mg) ferrite–wax composite in X-band frequencies. *Journal of Magnetism and Magnetic Materials, 320*(6), 864-870. doi:http://dx.doi.org/10.1016/j.jmmm.2007.09.020

Castel, E., Josse, M., Roulland, F., Michau, D., Raison, L., & Maglione, M. (2009). In-situ formation of barium ferrite in iron-doped "tetragonal tungsten bronze": Elaboration of room temperature multiferroic composites. *Journal of Magnetism and Magnetic Materials, 321*(11), 1773-1777. doi:http://dx.doi.org/10.1016/j.jmmm.2009.02.010

Cheng, J. P., Zhang, X. B., Yi, G. F., Ye, Y., & Xia, M. S. (2008). Preparation and magnetic properties of iron oxide and carbide nanoparticles in carbon nanotube matrix. *Journal of Alloys and Compounds, 455*(1–2), 5-9. doi:http://dx.doi.org/10.1016/j.jallcom.2007.01.014

Choodamani, C., Nagabhushana, G. P., Ashoka, S., Daruka Prasad, B., Rudraswamy, B., & Chandrappa, G. T. (2013). Structural and magnetic studies of Mg(1−x)ZnxFe2O4 nanoparticles prepared by a solution combustion method. *Journal of Alloys and Compounds, 578*(0), 103-109. doi:http://dx.doi.org/10.1016/j.jallcom.2013.04.152

Choudhry, Q., Azhar Khan, M., Nasar, G., Mahmood, A., Shahid, M., Shakir, I., & Farooq Warsi, M. (2015). Synthesis, characterization and study of magnetic, electrical and dielectric properties of La1−xDyxCo1−yFeyO3 nanoparticles prepared by wet chemical route. *Journal of Magnetism and Magnetic Materials, 393*, 67-72. doi:http://dx.doi.org/10.1016/j.jmmm.2015.05.040

Cullity, B. D. (1978). *Elenent of X-ray Diffraction* (Vol. 2nd Edition). New York: Addision-Wesely

Fei, P., Wang, Q., Zhong, M., & Su, B. (2016). Preparation and adsorption properties of enhanced magnetic zinc ferrite-reduced graphene oxide nanocomposites via a facile one-pot solvothermal method. *Journal of Alloys and Compounds, 685*, 411-417. doi:http://dx.doi.org/10.1016/j.jallcom.2016.05.279

Feller, J. F., Bruzaud, S., & Grohens, Y. (2004). Influence of clay nanofiller on electrical and rheological properties of conductive polymer composite. *Materials Letters, 58*(5), 739-745. doi:http://dx.doi.org/10.1016/j.matlet.2003.07.010

Goldman, A. (1990). *Modern Ferrite Technology*. New York: Van Nostrand Reinhold.

Griffiths, P. R., and J. A. Dehaseth. (1986). *Fourier Transform Infrared Spectrosopy*. New York: Wiley.

Hannour, A., Vincent, D., Kahlouche, F., Tchangoulian, A., Neveu, S., & Dupuis, V. (2014). Self-biased cobalt ferrite nanocomposites for microwave applications. *Journal of Magnetism and Magnetic Materials, 353*, 29-33. doi:http://dx.doi.org/10.1016/j.jmmm.2013.10.010

Huang, Y., Li, N., Ma, Y., Du, F., Li, F., He, X., . . . Chen, Y. (2007). The influence of single-walled carbon nanotube structure on the electromagnetic interference shielding efficiency of its epoxy composites. *Carbon, 45*(8), 1614-1621. doi:http://dx.doi.org/10.1016/j.carbon.2007.04.016

Ishaque, M., Islam, M. U., Azhar Khan, M., Rahman, I. Z., Genson, A., & Hampshire, S. (2010). Structural, electrical and dielectric properties of yttrium substituted nickel ferrites. *Physica B: Condensed Matter, 405*(6), 1532-1540. doi:http://dx.doi.org/10.1016/j.physb.2009.12.035

Jiang, J., Li, L., & Xu, F. (2007). Polyaniline–LiNi ferrite core–shell composite: Preparation, characterization and properties. *Materials Science and Engineering: A, 456*(1–2), 300-304. doi:http://dx.doi.org/10.1016/j.msea.2006.11.143

Kammer Hansen, K. (2013). Electrochemical reduction of oxygen and nitric oxide at low temperature on La1−xSrxMnO3+δ cathodes. *Materials Research Bulletin, 48*(9), 3274-3277. doi:http://dx.doi.org/10.1016/j.materresbull.2013.05.029

Kim, T., & Shima, M. (2007). Reduced magnetization in magnetic oxide nanoparticles. *Journal of Applied Physics, 101*(9), 09M516. doi:doi:http://dx.doi.org/10.1063/1.2712825

Li, L., Jiang, J., & Xu, F. (2007). Synthesis and ferrimagnetic properties of novel Sm-substituted LiNi ferrite–polyaniline nanocomposite. *Materials Letters, 61*(4–5), 1091-1096. doi:http://dx.doi.org/10.1016/j.matlet.2006.06.061

Li, L., Qiu, H., Wang, Y., Jiang, J., & Xu, F. (2008). Preparation and magnetic properties of Cu0.4Zn0.6Cr0.5Sm0.06Fe1.44O4/polyaniline nanocomposites. *Journal of Rare Earths, 26*(4), 558-562. doi:http://dx.doi.org/10.1016/S1002-0721(08)60136-2

Mirzaee, S., Farjami Shayesteh, S., & Mahdavifar, S. (2014). Anisotropy investigation of cobalt ferrite nanoparticles embedded in polyvinyl alcohol matrix: A Monte Carlo study. *Polymer, 55*(16), 3713-3719. doi:http://dx.doi.org/10.1016/j.polymer.2014.06.039

Nasar, G., Khan, M. A., Warsi, M. F., Shahid, M., Khalil, U., & Khan, M. S. (2016). Structural and electromechanical behavior evaluation of polymer-copper nanocomposites. *Macromolecular Research, 24*(4), 309-313. doi:10.1007/s13233-016-4043-3

Patil, R. P., Jadhav, B. V., & Hankare, P. P. (2013). Electrical and thermoelectric properties of nanocrystalline Mn-substituted lithium ferrites. *Results in Physics, 3*(0), 214-218. doi:http://dx.doi.org/10.1016/j.rinp.2013.09.006

Qi, T., Huang, C., Yan, S., Li, X.-J., & Pan, S.-Y. (2015). Synthesis, characterization and adsorption properties of magnetite/reduced graphene oxide nanocomposites. *Talanta, 144*, 1116-1124. doi:http://dx.doi.org/10.1016/j.talanta.2015.07.089

Rinkevich, A. B., Korolev, A. V., Samoylovich, M. I., Klescheva, S. M., & Perov, D. V. (2016). Magnetic properties of nanocomposites based on opal matrices with embedded ferrite-spinel nanoparticles. *Journal of Magnetism and Magnetic Materials, 399*, 216-220. doi:http://dx.doi.org/10.1016/j.jmmm.2015.09.068

Salafsky, J. S. (1999). Exciton dissociation, charge transport, and recombination in ultrathin, conjugated polymer-${\mathrm{TiO}}_{2}$ nanocrystal intermixed composites. *Physical Review B, 59*(16), 10885-10894.

Sankara Rao, B., Sunandana, C. S., Srikanth, V. V. S. S., Rao, T. N., Jain, P. K., Rajendran, T. V., & Jaisankar, V. (2015). International Conference on Nano Science & Engineering Application (ICONSEA-2014) Centre For Nano Science and TechnologyPreparation, Characterisation and Conductivity studies of Supramolecular polymer/Ferrite Nanocomposites. *Materials Today: Proceedings, 2*(9), 4421-4428. doi:http://dx.doi.org/10.1016/j.matpr.2015.10.043

Seo, M.-K., Rhee, K.-Y., & Park, S.-J. (2011). Influence of electro-beam irradiation on PTC/NTC behaviors of carbon blacks/HDPE conducting polymer composites. *Current Applied Physics, 11*(3), 428-433. doi:http://dx.doi.org/10.1016/j.cap.2010.08.013

Singh, N., Agarwal, A., & Sanghi, S. (2011). Dielectric relaxation, conductivity behavior and magnetic properties of Mg substituted Zn–Li ferrites. *Current applied physics, 11*(3), 783-789. doi:10.1016/j.cap.2010.11.073

Soibam, I., Phanjoubam, S., Sharma, H. B., Sarma, H. N. K., & Prakash, C. (2009). Magnetic studies of Li–Zn ferrites prepared by citrate precursor method. *Physica B: Condensed Matter, 404*(21), 3839-3841. doi:http://dx.doi.org/10.1016/j.physb.2009.07.107

Srivastava, M., Ojha, A. K., Chaubey, S., Sharma, P. K., & Pandey, A. C. (2010). Influence of pH on structural morphology and magnetic properties of ordered phase cobalt

doped lithium ferrites nanoparticles synthesized by sol–gel method. *Materials Science and Engineering: B, 175*(1), 14-21. doi:http://dx.doi.org/10.1016/j.mseb.2010.06.005

Srivastava, M., Singh, J., Mishra, R. K., Singh, M. K., Ojha, A. K., Yashpal, M., & Sudhanshu, S. (2014). Novel conducting lithium ferrite/chitosan nanocomposite: Synthesis, characterization, magnetic and dielectric properties. *Current Applied Physics, 14*(7), 980-990. doi:http://dx.doi.org/10.1016/j.cap.2014.04.013

Varshney, S., Singh, K., Ohlan, A., Jain, V. K., Dutta, V. P., & Dhawan, S. K. (2012). Synthesis, characterization and surface properties of Fe2O3 decorated ferromagnetic polypyrrole nanocomposites. *Journal of Alloys and Compounds, 538*, 107-114. doi:http://dx.doi.org/10.1016/j.jallcom.2012.05.119

Yinglin, X., Xiaomin, L., Jiantao, Z., Kaixue, W., Yong, G., Bo, L., . . . Xuefeng, Q. (2014). CoFe2O4-graphene Nanocomposites Synthesized through An Ultrasonic Method with Enhanced Performances as Anode Materials for Li-ion Batteries. *Nano-Micro Letters, 6*(4). doi:10.1007/s40820-014-0003-7